Journal of Materials Chemistry A

Accepted Manuscript

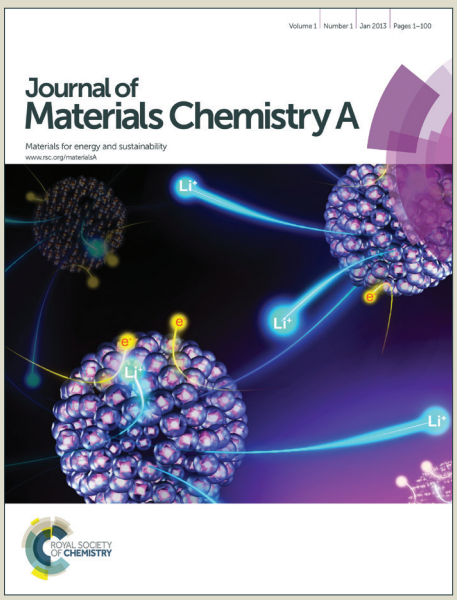

ROYAL SOCIETY OF CHEMISTRY

www.rsc.org/materialsA

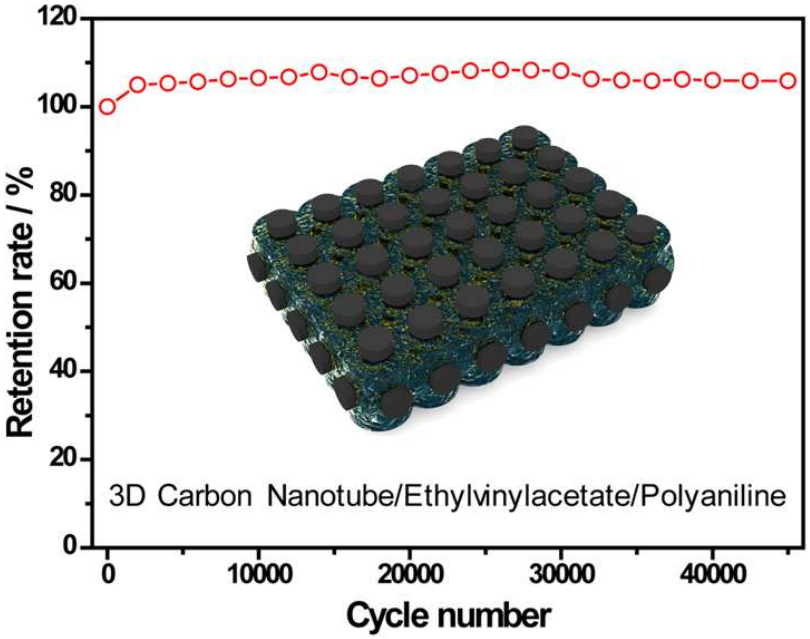

Journal of
Materials Chemistry A

RSCPublishing

COMMUNICATION

Three-Dimensional Carbon Nanotube/Ethylvinylacetate/Polyaniline as High Performance Electrode for Supercapacitor

Cite this: DOI: 10.1039/x0xx00000x

Received 00th January 2014,
Accepted 00th January 2014

DOI: 10.1039/x0xx00000x

www.rsc.org/MaterialsA

Zishou Zhang*,[a] Yangfan Zhang,[a] Kang Yang,[a] Kongyang Yi,[a] Zihui Zhou,[a] Aiping Huang,[a] Kancheng Mai,[a] and Xihong Lu[a]

In this work, an ultrahigh stable polyaniline that retained 100% of its initial capacitance after 45000 cycles was developed by designed and fabricated a ternary composite carbon nanotube/ ethylvinylacetate/ polyaniline (PANI/CNT/EVA) with 3D co-continuous phase structure. The areal specific capacity of PANI/CNT/EVA increased with the thickness increasing. These findings hold great promise for enlighten a broad area of shape-conformability energy-storage devices.

The rapid development of wearable and portable electronics have made flexible energy storage an important prerequisite.[1-3] In recent years, increasing efforts have been devoted to studying flexible storage devices like Li-ion batteries[4-6] and supercapacitors (SCs). SCs, also known as electrochemical capacitors, are considered to be a state-of-the art energy storage device due to its higher power density, relatively larger energy density and superior cycle lifetime.[4, 7-10] For high-performance flexible SCs, the electrodes applied in have become extremely important. Polyaniline (PANI), known as a promising pseudocapacitive electrode materials for supercapacitors[11-12], has been extensively studied due to their low cost, high electrical conductivity in doped states (~100-10000 S m^{-1}), [13-14] and ease of fabrication for large-scale devices. [15-17] It exhibits excellent specific capacitance of around 500 to 3400 F g^{-1}, which is substantially higher than metal oxide electrodes (about 300 to 1200 F g^{-1}).[18-22] However, the PANI experiences a large volumetric swelling and shrinking during charge/discharge process because of ion doping and dedoping, which will result in the structural breakdown and thus fast capacitance decay of conducting polymers.[23] Up to now, most of reports about PANI electrodes are not more than 80% retention after cycling for 1000 times.[24-28] Therefore, the poorly cycling performance is still a major obstacle for practical applications of PANI. Polymer composites with high capacitance stand for a new type of electrodes materials for supercapacitors of practical importance. It integrates unique properties such as light and small units, flexible, stretchable, shapeable and excellent mechanical properties of individual polymers into the high electrochemical active electrodes.[29-31] Moreover, the composites possess the common characteristics of polymers like the easy of processing ability for shape-conformability, while maintaining the uniqueness such as low cost, light weight, and multi- functionalization in comparison with conventional single polymer component.[32-33] This type of polymer composites has received increasing attention as novel current collectors. Tsuyoshi et al.[34] dispersed 20 wt% single-walled carbon nanotubes in a vinylidene fluoride-hexafluoropropylene copolymer matrix to form a rubber-like composite film with conductivity of 57 S cm^{-1} and a stretchability of 134%. Seisuke et al.[35] reported a highly conductive elastomeric composite with conductivity of 30 S cm^{-1} and excellent mechanical durability (4 500 strain cycles until failure), which was fabricated with polydimethylsiloxane filled by long single-walled carbon nanotubes with high aspect ratio and small diameter. Our previous work[36] used the mixture of CNT and carbon black filling ethylene-vinyl acetate copolymer (EVA) to act as flexible current collectors, which was deposited MnO_2 on the surface to fabricate flexible electrodes materials existed excellent electrochemical properties. However, these polymer composites still worked as 2D flat electrode and the materials inside the polymer composites cannot be utilized. The construction of co-continuous 3D polymer composites with good mechanical and electrochemical properties is still a challenge.

In this work, we designed and fabricated a ternary composite (PANI/CNT/EVA) with 3D co-continuous phase structure to act as polymer composite electrode materials for supercapacitors. The CNT/EVA with 3D co-continuous phase structure was synthesized by EVA filled with 40wt% CNT, and it has low cost, high conductivity (19.6 S cm^{-1}), excellent mechanical properties (tensile strength about 22.5 MPa and elongation at break about 55%, Figure S1, SI) great flexibility and even potential to model specific-shape (Figure 1a). The as synthesized PANI can integrate into the continuous network of CNT/EVA, even into the intermolecular of EVA. The elasticity of the CNT/EVA can efficiently avoid the structural breakdown of the PANI during charge/discharge process. Significantly, the as-prepared EVA/CNT/PANI presented the amazing capacity retention of 100% after 45 000 cycles, which is considerably the highest performance of PANI based electrodes

reported recently. Moreover, the areal specific capacity of PANI/CNT/EVA was 1738.3 mF cm^{-2} for about 0.8 mm thickness at the current density of 2 mA cm^{-2}.

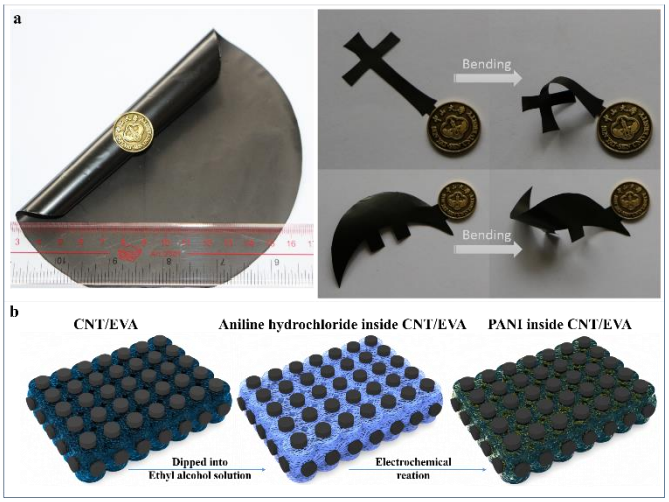

Figure 1. (a) Photo images of 40% CNT/EVA. (b) Schematic diagram of the manufacturing processes of ternary composite with co-continuous phase structure.

The ternary composite (PANI/CNT/EVA) with 3D co-continuous phase structure was synthesized by a two-step process (see Method in Supporting Information, SI), as illustrated in Figure 1b. Given that the aniline hydrochloride is easily dissolved in ethyl alcohol (Figure S2, SI), the CNT/EVA composite were dipped into the ethyl alcohol solution containing aniline hydrochloride and then took out to volatilize ethyl alcohol completely. Therefore the aniline hydrochloride can stay inside CNT/EVA composite to act as working electrode. Finally, the continuous PANI network around CNT (denoted as PANI/CNT/EVA) was obtained via adopting working electrode in a conventional three-electrode cell by CV techniques (Experimental Section). 40wt%CNT/EVA with highest conductivity absorbed aniline hydrochloride at 70 °C to form PANI/CNT/EVA in 0.3 M H_2SO_4 by CV techniques with 50 cycles of scan rating 50 mV s^{-1} from 0 to 1V, and it was donoted as 0.3mm-PANI/CNT/EVA. Brunner-Emmet-Teller (BET) measurements results are shown in Figure 2 and Table 1. The total pore volume of CNT/EVA and PANI/CNT/EVA are 0.02 and 0.10 cm^3 g^{-1}, respectively, indicating that the PANI/CNT/EVA form a more porous structure than CNT/EVA. Scanning Electron Microscope (SEM) images of the surface (Figure 3a, b) and cross-section (Figure 3c, d) also confirmed the upper results. Clearly, the nanofibers of PANI/CNT/EVA became thicker than that of CNT/EVA, indicating that the PANI successfully coated on the CNT/EVA. The transmission electron microscopy (TEM) images indicated that the average diameter of nanofibers of PANI/CNT/EVA (~15 nm) is similar to that of the CNT/EVA sample (Figure S3, SI). To confirm the PANI coating on the whole 3D CNT/EVA network, the atomic force microscope (AFM) phase images are shown in Figure 3e, f, and the relative height images are shown in Figure S4, SI. In comparison to the results of CNT/EVA, It can be seen that the intertwining network of co-continuous phase structure was preserved in PANI/CNT/EVA, while some particles with irregular form were fabricated around and even inserted into the nanofibers, and the structure of three phases were found in these regions.

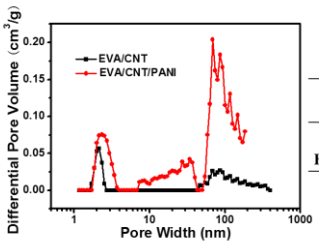

Table 1. Pore parameters

sample	BET surface area(m^2 g^{-1})	Total pore volume(cm^3 g^{-1})
EVA/CNT	30	0.02
EVA/CNT/PANI	46	0.10

Figure 2. DFT pore size distribution of CNT/EVA and PANI/CNT/EVA.

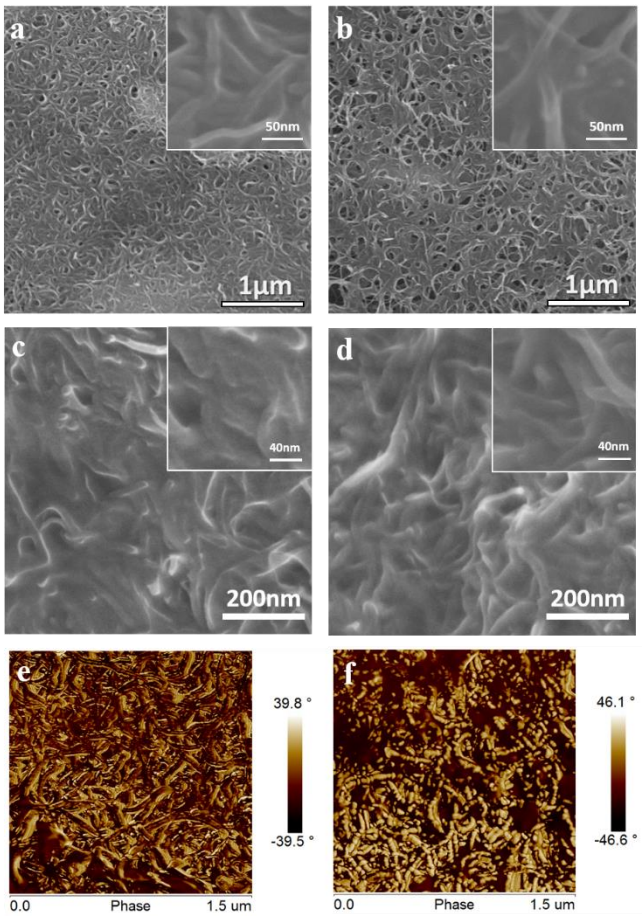

Figure 3. The surface SEM image of (a) CNT/EVA and (b) PANI/CNT/EVA. The cross-sectional SEM image of (c) CNT/EVA and (d) PANI/CNT/EVA. The AFM phase image of (e) CNT/EVA and (f) PANI/CNT/EVA.

To further confirm the possible phase and compositions, we performed FT-IR, X-ray diffraction (XRD) and X-ray photoelectron spectroscopy (XPS) analysis on the PANI/CNT/EVA and CNT/EVA composites. The FT-IR spectra (Figure 4a) presents that the characteristic absorption peak of PANI, C-N stretching of secondary aromatic amines at 1305 cm^{-1}, is observed in 0.3mm-PANI/CNT/EVA while inexistence in 40wt% CNT/EVA composites. Meanwhile, the X-ray photoelectron spectroscopy (XPS) spectrum reveals N1s at 400.7 eV existed in 0.3mm-PANI/CNT/EVA (Figure S5, SI). These results confirmed the occurrence of PANI in CNT/EVA after electrochemical reactions. The as-fabricated PANI has amorphous nature which was revealed by X-ray diffractometer (XRD) analysis results shown in Figure 3b. All diffraction peaks can be attributed to EVA and CNT. Two peaks at 8.3 °

and 14.6 ° exhibited in CNT/EVA while disappeared in PANI/CNT/EVA composites are originated from the crystallization of EVA.[37-38] These result indicates that the as-fabrication PANI was inserted into the intermolecular of EVA resulting in some part of crystalline region of EVA damaged, which were consistent with the results of AFM measurements shown above. Based on the detailed analysis mentioned above, it can be concluded that PANI network was fabricated in 3D CNT/EVA network to form co-continuous phase structure of ternary composite (PANI/CNT/EVA).

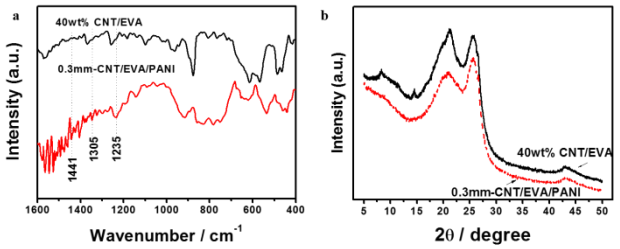

Figure 4. (a) FT-IR spectra and (b) XRD spectra of 40wt% CNT/EVA and 0.3mm-PANI/CNT/EVA.

To evaluate the electrochemical performance of the PANI/CNT/EVA electrode, electrochemical measurements were conducted in a three-electrode cell using 1 M H_2SO_4 aqueous solution as the electrolyte with a Pt wire counter electrode and a saturated calomel electrode (SCE) reference electrode. Figure 5a compares the CV curves of PANI/CNT/EVA and CNT/EVA electrodes collected at a scan rate of 20 mV/s. Obviously, the PANI/CNT/EVA electrode exhibits a substantially larger current density than CNT/EVA, indicating its excellent capacitive performance. The CV curves collected at varied scan rates (5 ~ 100 mV s^{-1}) are presented in Figure 5b. The redox peaks observed in CV curves can be attributed to the redox transition of PANI between a semiconducting state (leucoemeraldine form) and a conducting state (polaronic emeraldine form) and transformation of emeraldine-pernigraniline.[39] Moreover, the good symmetrical characteristics of the anodic and cathodic peaks indicate the good redox reversibility of the PANI/CNT/EVA electrode. Based on the CV curves, the areal capacitance and specific capacitance were calculated (details see Experimental section) and plotted as a function of scan rates in Figure 5c. Clearly, the PANI/CNT/EVA electrode yields a high areal capacitance of 575 mF cm^{-2} and a specific capacitance of 1106 F g^{-1} at scan rate of 5 mV s^{-1}, which are substantially higher than those of recently reported PANI based electrode, such as PANI nanotubes (860 F g^{-1}), [40] RGO/PANI (553 F g^{-1}), [41] SLS/MWCNTs/PANI (401 F g^{-1}), [42] RGO/CNT/PANI (747 F g^{-1}) [43] and PANI/CNT/PDMS (1023 F g^{-1}).[32] Moreover, a good rate capability of 25.7% retention is achieved as the scan rates increases from 5 to 100 mV s^{-1}. This outstanding electrochemical performance of the PANI/CNT/EVA electrode can be ascribed to the good conductivity and high surface area of 3D CNT/EVA support and the firmly integration of PANI to 3D CNT/EVA support.

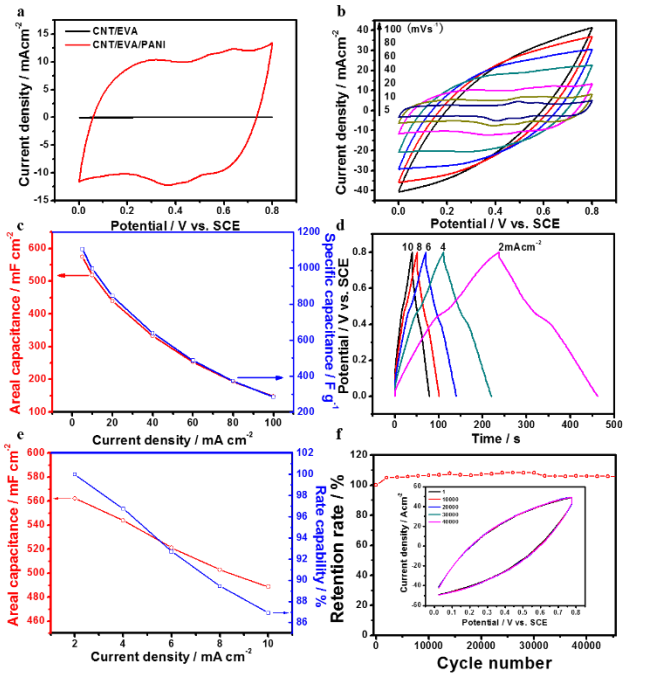

Figure 5. (a) CV curves of 40wt% CNT/EVA and 0.3mm-PANI/CNT/EVA electrodes collected at 20 mV s^{-1}. (b) CV curves and of 0.3 mm-PANI/CNT/EVA electrode collected at different scan rate. (c) Areal and specific capacitance as a function of scan rate and current density of 0.3mm-PANI/CNT/EVA electrode. (d) Galvanostatic charge-discharge curves of 0.3mm-PANI/CNT/EVA electrode collected at different current density. (e) Areal capacitance and rate capability as a function of different current densities. (f) Cycle stability of 0.3mm-PANI/CNT/EVA electrode during the long-term CV process at 200 mV s^{-1}. Inset showing the corresponding CV curves.

The galvanostatic charge-discharge measurements were carried out at different current densities from 2 to 10 mA cm^{-2} to further confirm the outstanding capacitive performance. Figure 5d shows the galvanostatic charge/discharge curves of PANI/CNT/EVA electrode. All curves at different current densities exhibited almost the same shape, almost triangular shape in the potential range from 0 to 0.8 V vs. SCE. It means that PANI/CNT/EVA possessed the reversible behavior of the ideal capacitor, which was sustainable in a broad current density range. Significantly, a high areal capacitance of 562.3 mF cm^{-2} has been obtained by PANI/CNT/EVA at 2 mA cm^{-2}, which is considerably higher than that of recently reported PANI based electrodes, such as CNT@PANI yarn (38 mF cm^{-2} at 0.01 mA cm^{-2})[44], PANI/G (355.6 mF cm^{-2} at 0.5 mA cm^{-2})[45], PANI/GO (19.2 mF cm^{-2} at 0.008 mA cm^{-2})[46], CNF paper/PANI/RGO (5.86 mF cm^{-2} at 0.0043 mA cm^{-2})[47]. It also exhibits an excellent rate capability with 86.9% retention of the initial capacitance as the current density increases from 2 to 10 mA cm^{-2}. This outstanding capacitance and rate capability can be attributed to the unique structural features of PANI/CNT/EVA: (1) 3D continuous network of PANI with high accessible surface area for electrolytes and high conductivity (coated on the surface of CNT). (2) The firmly integration of PANI to 3D CNT/EVA support with elasticity.

The cycling performance, another important index for electrode materials as supercapacitors, was shown from the areal capacitance as a function of cycle numbers based on CV curves at the scan rate of 200 mV s^{-1} (Figure 5f) for 45000

cycles. It was noted that the areal capacitance of 0.3mm-PANI/CNT/EVA was sustainable before 45 000 cycles, still retaining 100% of its initial cycle. Thus, the cycling performance of continuous PANI network in 40wt% CNT/EVA is fairly good for ideal supercapacitors, which are substantially higher than those of recently reported PANI based electrode, such as PANI@C (capacitance retentions of 95% after 10000 cycles), [48] graphene-PANI (capacitance retentions of 82% after 1000 cycles) [49] and PANI/CNT/PDMS (capacitance retentions of 95.6% after 500 cycles) [32]. The superior capacitive behavior of 0.3mm-PANI/CNT/EVA electrodes can be attributed to (1) the direct connection between electrochemically active PANI with CNT in CNT/EVA can effectively facilitate the interfacial charge transfer; (2) PANI integrated into the continuous structure or even the intermolecular of CNT/EVA, which can not only significantly increases the accessible surface area as well as active sites for redox reaction, but also prevent the PANI from structure pulverization.

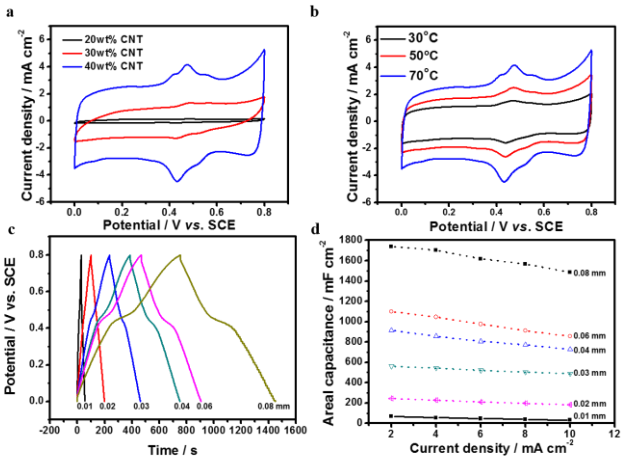

Figure 6. (a) CV curves (scan rate of 5 mV s^{-1}) of CNT/EVA contained different CNT absorbed aniline hydrochloride at 70 °C to fabricate PANI/CNT/EVA, and (b) CV curves (scan rate of 5 mV s^{-1}) of 40wt% CNT/EVA absorbed aniline hydrochloride at different temperature to fabricate PANI/CNT/EVA. The detailed parameter of cyclic voltammetry method is: scan rates (50 mV s^{-1}), potential range (0 – 1 V), 50 cycles and electrolyte solution (0.3 M H_2SO_4). (c) Galvanostatic charge–discharge curves of PANI inside various thickness of CNT/EVA at the current density of 2 mA cm^{-2}. (d) Variation of areal capacitance with current density for PANI inside various thickness of 40wt% CNT/EVA.

To investigate the correlation between the contents of three components and the electrochemical property, PANI/CNT/EVA composites contained different CNT and PANI were obtained by varying the contents of CNT and synthesis of PANI under different parameters. The CV curves (Figure 6a) of CNT/EVA/PANI synthesis from CNT/EVA with different content of CNT under the same parameters showed that the current density was increased with the content of CNT increasing, and the calculated areal capacitances (Figure S6, SI) confirmed that 40wt%CNT/EVA/PANI had highest capacity. To change the content of PANI in CNT/EVA/PANI, various synthesis parameters and the temperature of CNT/EVA absorbed the ethyl alcohol solution of aniline hydrochloride were optimized to fabricate 40wt%CNT/EVA/PANI (Figure 7-10, SI). The results (Figure 6b) indicated that the capacity of PANI/CNT/EVA was increased with the content of PANI. Moreover, the PANI/CNT/EVA with the highest capacity can be fabricated by 40wt%CNT/EVA absorbed aniline hydrochloride at 70 °C to form PANI/CNT/EVA in 0.3 M H_2SO_4 by CV techniques with 50 cycles of scan rating 50 mV s^{-1} from 0 to 1V. On the other hand, various thick sheets of 40wt% CNT/EVA with 0.5*2.5 cm^2 were used to fabricate working electrodes as the above analyzed 0.3mm-PANI/CNT/EVA. Figure 6c shows the galvanostatic charge-discharge curves of PANI inside various thickness of 40wt% CNT/EVA at the current density of 2 mA cm^{-2}. The approximately linear and symmetrical charge-discharge curves confirms that continuous PANI inside various thickness of 40wt% CNT/EVA has good coulombic efficiency and excellent reversibility. It can be found that the discharge times of PANI inside 40wt% CNT/EVA was extension from 27.4 seconds to 696.1 seconds with the thickness of CNT/EVA increasing from about 0.1 to 0.8 mm at the current density of 2 mA cm^{-2}. The corresponding areal capacity shown in Figure 6d increased from 68.5 mF cm^{-2} to 1738.3 mF cm^{-2}. Although it's hard to obtain thicker 40wt% CNT/EVA over 0.8 mm by solution method, the results largely indicated that the capacity of the as-prepared PANI/CNT/EVA is determined by the volume of the current collector, 40wt% CNT/EVA.

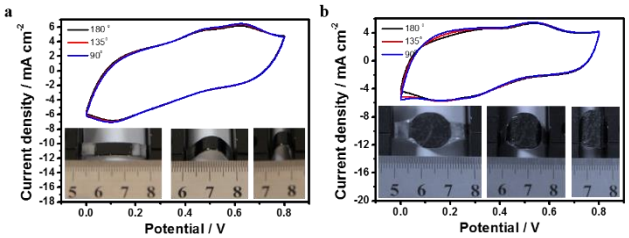

Figure 7. CV curves of the prepared solid-state SC device collected at a scan rate of 10 mV s^{-1} in different bending states. Inset: bending the device.

To test their feasibility for application as a flexible energy storage device, solid-state symmetrical SCs based on PANI/CNT/EVA were fabricated by sandwiching PVA/H_2SO_4 based solid-state electrolyte and filter paper between two pieces of elongated or rounded PANI/CNT/EVA electrodes with 1 cm^2 (Figure 7). The as-fabricated solid-state SCs have similar capacitance and excellent flexibility, and they can undergo blending and twisting. More importantly, the electrochemical behaviour of the as-fabricated SC devices have no significant change under various bending angles, further confirming that the devices have remarkable mechanical flexibility. These results convincingly show that ternary composite (PANI/CNT/EVA) with co-continuous phase structure for shape-conformability supercapacitor with high performances can be realized in the method of this work.

Conclusions

In summary, a kind of 40wt% CNT/EVA composite with low cost, excellent conductivity of 19.6 S cm^{-1}, good mechanical properties of 50% elongation at break and co-continuous phase structure was developed and acted as framework and current collector to fabricate ternary composite (PANI/CNT/EVA) with co-continuous phase structure for shape-conformability supercapacitor. When using 0.3 mm thickness of 40wt% CNT/EVA support for electrochemically active PANI with continuous network, the 0.3mm-PANI/CNT/EVA electrode achieved a high areal capacitance of 575 mF cm^{-2} and specific

capacitance of 1105 F g^{-1} at a scan rate of 5 mV s^{-1}. More importantly, continuous PANI inside 40wt% CNT/EVA presented an amazing cycling performance of sustainable during 45 000 cycles, and the capacitance of PANI/CNT/EVA was relied on the thickness of 40wt% CNT/EVA, thicker 40wt% CNT/EVA higher capacitance. Based on the common characteristics of polymers and their co-continuous phase structure, such high performance of PANI/CNT/EVA electrode makes them very promising in design and fabrication of shape-conformability supercapacitors. All these findings are expected to enlighten a broad area of shape-conformability energy-storage devices.

Acknowledgements

We acknowledge the support of this work by the Natural Science Foundations of China (51303215), the Research Fund for the Doctoral Program of Higher Education of China (20110171120018).

Notes and references

[a] MOE of Key Laboratory for Polymeric Composite and Functional Materials, Guangdong Provincial Key Laboratory for High Performance Polymer-based Composites, School of Chemistry and Chemical Engineering, Sun Yat-Sen University, Guangzhou 510275, People's Republic of China.

*Contact information for corresponding authors:

135 Xingang West Road, Institute of Materials Science 306, Guangzhou, 510275 China Phone: 86-20-84115109 Fax: 86-20-84115109. Email: zhzish@mail.sysu.edu.cn (Z. S. Zhang)

Electronic Supplementary Information (ESI) available: [details of any supplementary information available should be included here]. See DOI: 10.1039/c000000x/

1 J. Ge, G. H. Cheng and L.W. Chen, *Nanoscale*, 2011, **3**, 3084–3088.
2 X. Lu, G. Wang, T. Zhai, M. Yu, S. Xie, Y. Ling, C. Liang, Y. Tong and Y. Li, *Nano lett.*, 2012, **12,** 5376-5381.
3 C. Z. Yuan, L. Yang, L. R. Hou, L. F. Shen, X. G. Zhang and X. W. Lou, *Energy Environm. Sci.*, 2012, **5**, 7883-7887.
4 J. Xiao and S. Yang, *RSC Advances*, 2011, **1**, 588-595.
5 L. Yuan, X. Xiao, T. Ding, J. Zhong, X. Zhang, Y. Shen, B. Hu, Y. Huang, J. Zhou and Z. L. Wang, *Angewandte Chemie*, 2012, **124**, 5018-5022.
6 T. Zhai, F. Wang, M. H. Yu, S. Xie, C. Liang, C. Li, F. Xiao, R. Tang, Q. Wu and X. H. Lu, *Nanoscale*, 2013, **5**, 6790-6796.
7 M. K. Liu, Y. E. Miao, C. Zhang, W. W. Tjiu, Z. B. Yang, H. S. Peng and T. X. Liu, *Nanoscale*, 2013, **5**, 7312–7320.
8 B. G. Choi, S.-J. Chang, H.-W. Kang, C. P. Park, H. J. Kim, W. H. Hong, S. Lee and Y. S. Huh, *Nanoscale*, 2012, **4**, 4983-4988.
9 X. Lu, M. Yu, G. Wang, T. Zhai, S. Xie, Y. Ling, Y. Tong and Y. Li, *Adv. Mater.*, 2013, **25**, 267-272.
10 B. G. Choi, J. Hong, W. H. Hong, P. T. Hammond and H. Park, *ACS nano*, 2011, **5**, 7205-7213.
11 X. B. Yan, Z. X. Tai, J. T. Chen and Q. J. Xue, *Nanoscale*, 2011, **3**, 212–216.
12 A. Ghosh and Y. H. Lee, *ChemSusChem*, 2012, **5**, 480-499.
13 H. Zengin, W. Zhou, J. Jin, R. Czerw, D. W. Smith, L. Echegoyen, D. L. Carroll, S. H. Foulger and J. Ballato, *Adv. Mater.*,2002, **14**, 1480-1483.
14 M. Massi, C. Albonetti, M. Facchini, M. Cavallini and F. Biscarini, *Adv. Mater.*, 2006, **18**, 2739-2742.
15 H. P. Cong, X. C. Ren, P. Wang and S. H. Yu, *Energy Environ. Sci.*, 2013, **6**, 1185-1191.
16 C. O. Baker, B. Shedd, R. J. Tseng, A. A. Martine-Morales, C. S. Ozkan, M. Ozkan, Y. Yang and R. B. Kaner, *ACS Nano*, 2011, **5**, 3469–3474.
17 K. Wang, Q. H. Meng, Y. J. Zhang, Z. X. Wei and M. H. Miao, *Adv. Mater.*, 2013, **25**, 1494-1498.
18 K. Y. Xie, J. Li, Y. Q. Lai, Z. A. Zhang, Y. X. Liu and G. G. Zhang, H. T. Huang, *Nanoscale*, 2011, **3**, 2202–2207.
19 M. J. Zhi, C. C. Xiang, J. T. Li, M. Li and N. Q. Wu, *Nanoscale*, 2013, **5**, 72–88.
20 M. Q. Xue, F. W. Li, J. Zhu, H. Song, M. N. Zhang and T. B. Cao, *Adv. Funct. Mater.*, 2012, **22**, 1284-1290.
21 C. Peng, D. Hu and G. Z. Chen, *Chem. Commun.*, 2011, **47**, 4105-4107.
22 J. Jiang, Y. Y. Li, J. P. Liu, X. T. Huang, C. Z. Yuan and X. W. Lou, *Adv. Mater.*, 2012, **24**, 5166-5180.
23 T. Y. Liu, L. Finn, M. H. Yu, H. Y. Wang, T. Zhai, X. H. Lu, Y. X. Tong and Y. Li, *Nano Lett.*, 2014, **14**, 2522–2527.
24 G. A. Snook, P. Kao and A. S. Best, *J. Power Sources*, 2011, **196**, 1-12.
25 H. L. Wang, Q. L. Hao, X. J. Yang, L. D. Lu and X. Wang, *Nanoscale*, 2010, **2**, 2164–2170.
26 S. Q. Jiao, J. G. Tu, C. Y. Fan, J. G. Hou and D. J. Fray, *J. Mater. Chem.*, 2011, **21**, 9027-9030.
27 K. Y. Xie, J. Li, Y. Q. Lai, Z. A. Zhang, Y. X. Liu, G. G. Zhang and H. T. Huang, *Nanoscale*, 2011, **3**, 2202-2207.
28 Y. Li, Y. Z. Fang, H. Liu, X. M. Wu and Y. Lu, *Nanoscale*, 2012, **4**, 2867–2869.
29 X. L. Chen, H. J. Lin, P. N. Chen, G. Z. Cuan, J. Deng and H. S. Peng, *Adv. Mater.*, 2014, **26**, 4444-4449.
30 X. Cai, M. Peng, X. Yu, Y. P. Fu and D. C. Zou, *J. Mater. Chem. C*, 2014, **2**, 1184–1200.
31 G. P. Hao, F. Hippauf, M. Oschatz, F. M. Wisser, A. Leifert, W. Nickel, N. Mohamed-Noriege, Z. Zheng and S. Kaskel, *ACS Nano*, 2014, **8**, 7138–7146.
32 M. H. Yu, Y. F. Zhang, Y. X. Zeng, B. Muhammad-Sadeeq, K. C. Mai, Z. S. Zhang, X. H. Lu and Y. X. Tong, *Adv. Mater.*, 2014, **26**, 4724-4729.
33 K. Wang, H. P. Wu, Y. N. Meng and Z. X. Wei, *Small*, 2014, **10**, 14–31.
34 T. Sekitani, Y. Noguchi, K. Hata, T. Fukushima, T. Aida and T. Someya, *Science*, 2008, **321**, 1468-1472.
35 S. Ata, K. Kobashi, M. Yumura and K. Hata, *Nano Lett.*, 2012, **12**, 2710-2716.
36 Z. S. Zhang, T. Zhai, X. H. Lu, M. H. Yu, Y. X. Tong and K. C. Mai, *J. Mater. Chem. A*, 2013, **1**, 505-509.
37 Q. Wang, Q. Yao, J. Chang and L. D. Chen, *J. Mater. Chem.*, 2012, **22**, 17612–17618.
38 W. A. Zhang, D. Z. Chen, Q. B. Zhao and Y. E. Fang, *Polymer*, 2003, **44**, 7953–7961.

39 X. M. Feng, R. M. Li, Y. W. Ma, R. F. Chen, N. E. Shi, Q. L. Fan and W. Huang, *Adv. Funct. Mater.*, 2011, **21**, 2989–2996.
40 Z. L. Wang, R. Guo, G. R. Li, H. L. Lu, Z. Q. Liu, F. M. Xiao, M. Q. Zhang and Y. X. Tong, *J. Mater. Chem.*, 2012, **22**, 2401-2404.
41 W. Chen, R. B. Rakhi and H. N. Alshareef, *Nanoscale*, 2013, **5**, 4134-4138.
42 M. Ammam and J. Fransaer, *Chem. Commun.*, 2012, **48**, 2036-2038.
43 J. Yan, T. Wei, Z. J. Fan, W. Z. Qian, M. L. Zhang, X. D. Shen and F. Wei, *J. Power Sources*, 2010, **195**, 3041-3045.
44 K. Wang, Q. H. Meng, Y. J. Zhang, Z. X. Wei and M. H. Miao, *Adv. Mater.*, 2013, **25**, 1494-1498.
45 B. Yao, L. Y. Yuan, X. Xiao, J. Zhang, Y. Y. Qi, J. Zhou, J. Zhou, B. Hu and W. Chen, *Nano Energy*, 2013, **2**, 1071–1078.
46 H. G. Wei, J. H. Zhu, S. J. Wu, S. Y. Wei and Z. H. Guo, *Polymer*, 2013, **54**, 1820-1831.
47 X. Wang, K. Z. Gao, Z. Q. Shao, X. Q. Peng, X. Wu and F. J. Wang, *J. Power Sources*, 2014, **249**, 148-155.
48 T. Y. Liu, L. Finn, M. H. Yu, H. Y. Wang, T, Zhai, X. H. Lu, Y. X. Tong and Y. Li, *Nano Lett.*, 2014, **14**, 2522–2527.
49 H. P. Cong, X. C. Ren, P. Wang and S. H. Yu, *Energy Environ. Sci.*, 2013, **6**, 1185–1191.

